Three-dimensional mixed-wet random pore-scale network modeling of two- and three-phase flow in porous media. II. Results

Mohammad Piri* and Martin J. Blunt
Department of Earth Science and Engineering, Imperial College, London SW7 2AZ, United Kingdom
(Received 26 July 2004; published 4 February 2005)

We use the model described in Piri and Blunt [Phys. Rev. E **71**, 026301 (2005)] to predict two- and three-phase relative permeabilities of Berea sandstone using a random network to represent the pore space. We predict measured relative permeabilities for two-phase flow in a water-wet system. We then successfully predict the steady-state oil, water, and gas three-phase relative permeabilities measured by Oak (Proceedings of the SPE/DOE Seventh Symposium on Enhanced Oil Recovery, Tulsa, OK, 1990). We also study secondary and tertiary gas injection into media of different wettability and initial oil saturation and interpret the results in terms of pore-scale displacement processes.

DOI: 10.1103/PhysRevE.71.026302 PACS number(s): 47.55.Mh, 68.08.Bc

I. INTRODUCTION

Prediction of three-phase relative permeabilities has been the aim of previous three-phase network modeling studies. Fenwick and Blunt [1,2] presented relative permeabilities for secondary and tertiary gas injection into different initial oil saturations. The resultant saturation paths compared well qualitatively with experimental data by Grader and O'Meara [3]. Oil relative permeabilities for different initial conditions were different from each other, consistent with several experimental studies [4–8]. Mani and Mohanty [9,10] studied the effect of spreading coefficient and saturation history on three-phase relative permeability and their results were consistent with other network modeling studies [1,2,11,12] and experimental measurements [4–8]. Van Dijke and coworkers [13–17] have studied qualitatively the saturation dependence of three-phase relative permeability. Lerdahl *et al.* [18] compared their simulated results successfully against the experimental data by Oak [4]. We will use a similar network in our studies (see Piri and Blunt [19]), and also compare our predictions against Oak's experiments [4]. In our study we will compare results on a point-by-point basis using our saturation tracking algorithm and extend the model to mixed-wet systems following the approach of Hui and Blunt [20].

II. COMPARISON WITH EXPERIMENT

The experiments we compare against will be two- and three-phase steady-state measurements of relative permeability performed by Oak on water-wet Berea sandstone [4]. The fluids used by Oak were dodecane with 10% iodooctane, brine, and air (nitrogen). Oak did not measure interfacial tensions. Pure dodecane-water-air systems have a negative spreading coefficient; however, it is known that the presence of even small amounts of other alkanes in the oil can affect the spreading behavior significantly [21]. The low oil saturations reached in Oak's experiments indicate a spreading system as assumed by other authors who have studied these data [18,22]. Consequently in this section we will use interfacial tensions for a spreading hexane-water-air system (Table I). These values are likely to be similar to those in the experiments—small changes in the interfacial tensions, as long as the system remains spreading, have a negligible impact on the results.

Oak studied three cores with permeabilities of 1000, 800, and 200 mD. Our network has a permeability of 3055 mD (see Table II in Ref. [19]). Oak found that the measured two-phase relative permeabilities for the least permeable core were different from the other two. In our study we will only compare against data from the two more permeable cores since their permeability and hence pore structure is likely to be more representative of our network.

A. Two-phase simulations: Primary drainage

During primary drainage, the receding contact angle is assumed to be 0°; in predicting Berea data there are no other parameters to adjust. Figure 1 shows the prediction against experimental data for oil-water, gas-oil, and gas-water drainage. The predictions are excellent and similar to those obtained using a two-phase network model by Valvatne and Blunt [24]. If we have a good representation of the pore structure and the displacement physics is straightforward, we can readily make reliable predictions.

B. Two-phase simulations: Imbibition

To predict imbibition data, we assumed a uniform distribution of advancing contact angles. In all cases the initial condition was an irreducible saturation of the wetting phase, with all possible pores and throats occupied by nonwetting

TABLE I. Interfacial tensions and spreading coefficient (mN/m) used in this work [20,23].

Fluids	σ_{ow}	σ_{go}	σ_{gw}	C_s
Hexane-water-air	48	19	67	0

*Electronic address: mpiri@princeton.edu

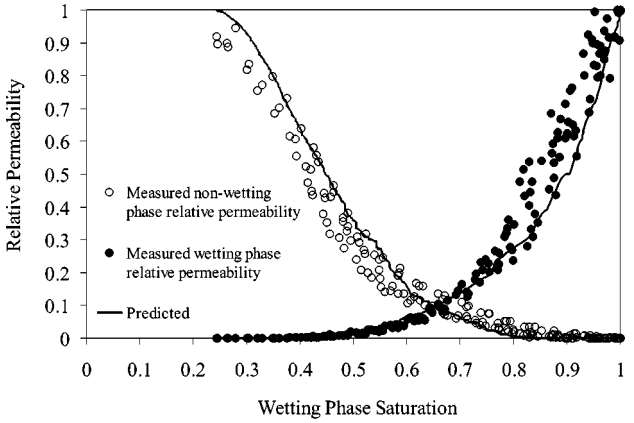

FIG. 1. Comparison of experimental [4] and predicted relative permeabilities during primary drainage in Berea sandstone.

phase at the end of primary drainage. Oak measured relative permeabilities for oil-water (water-wetting phase), gas-oil (oil-wetting phase), and gas-water (water-wetting phase) systems.

In imbibition there is a competition between pore-body filling and snapoff. A large aspect ratio (pores much larger than throats) and a low contact angle favors snapoff leading to a large trapped nonwetting phase saturation. As the contact angle increases, there is less trapping as the displacement is more connected [25,26]. We adjusted the range of contact angle to match the trapped nonwetting phase saturation at the end of imbibition. The advancing oil-water and gas-oil contact angles were in the range 63°–80° and 30°–70°, respectively. These values are representative of effective contact angles on microscopically rough surfaces [27,28]. Furthermore, we expect oil to be more wetting in the presence of gas than water in the presence of oil, since there are virtually no molecular interactions between gas and oil. The results are shown in Figs. 2 and 3. Small changes in the contact angle distribution did not adversely affect the match with experiment. With a representative range of contact angle we are able to predict relative permeabilities in imbibition.

As discussed in Sec. III in Ref. [19] in three-phase flow once two contact angles are known, the third can be predicted using the Bartell and Osterhoff equation [29]:

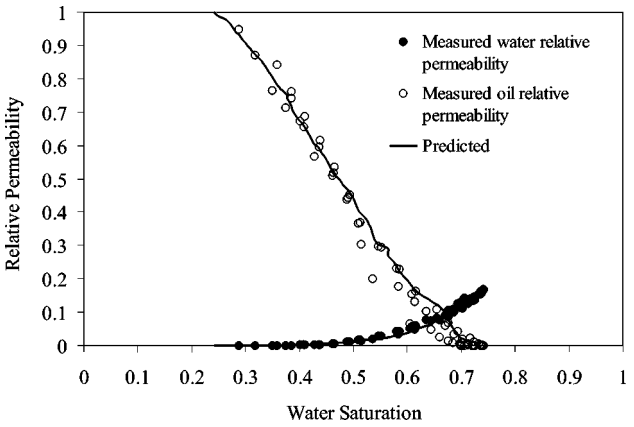

FIG. 2. Comparison of measured [4] and predicted oil-water two-phase relative permeabilities for imbibition in Berea sandstone.

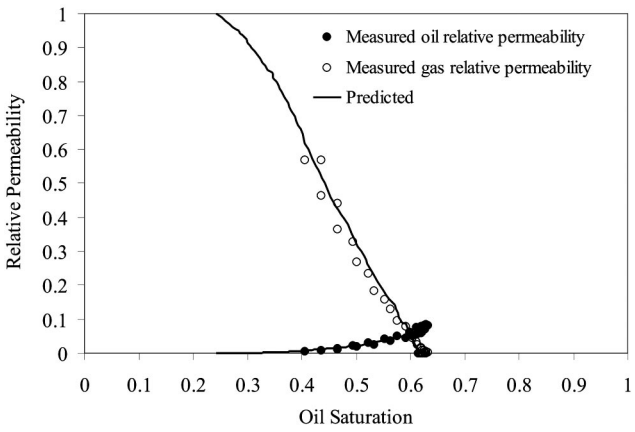

FIG. 3. Comparison of measured [4] and predicted two-phase gas-oil relative permeabilities for imbibition in Berea sandstone.

$$\sigma_{gw}^{eq} \cos \theta_{gw} = \sigma_{go}^{eq} \cos \theta_{go} + \sigma_{ow}^{eq} \cos \theta_{ow}. \quad (1)$$

Equation (1) was used to find the advancing gas-water contact angles from the advancing oil-water and gas-oil values and these were used in a simulation of water displacing gas. The advancing gas-water contact angles were distributed between 55.2° and 77.2°. Water in the presence of gas is less wetting than oil in gas, but more wetting than water in oil. The comparison of predicted and measured relative permeabilities is shown in Fig. 4. The predictions are excellent. In particular the residual gas saturation is accurately predicted.

C. Three-phase simulations

We will now predict three-phase relative permeability. We use the same advancing contact angles as for two-phase flow. We assume that the receding contact angles are 20° lower than the advancing values, which is a typical amount of hysteresis for water-wet media [28]. The contact angles used are given in Table II.

1. General behavior

Figure 5 shows a comparison of predicted three-phase oil relative permeability during gas injection with the measured

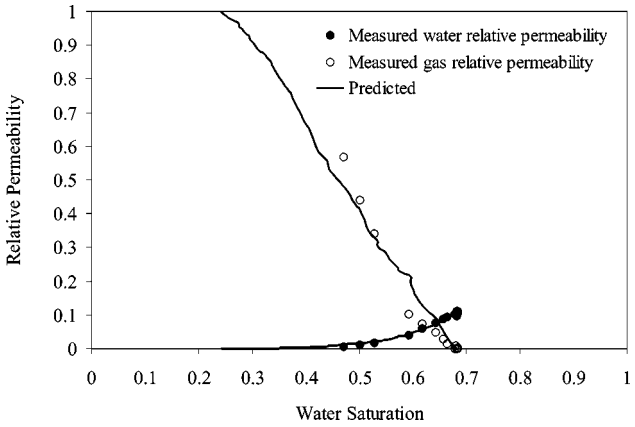

FIG. 4. Comparison of measured [4] and predicted two-phase gas-water relative permeabilities for imbibition in Berea sandstone.

TABLE II. Contact angles (degrees) used to predict the experiments.

$\theta_{ow}^{Primary\ Drainage\ (PD)}$	θ_{gw}^{PD}	θ_{ow}^{r}	θ_{ow}^{a}	θ_{go}^{r}	θ_{go}^{a}	θ_{gw}^{r}	θ_{gw}^{a}
0	0	43–60	63–80	10–50	30–70	36.6–57.3	55.2–77.2

steady-state values published by Oak [4]. The predicted results are produced by simulating tertiary gas injection into different initial oil saturations after water flooding maintaining a constant oil-water capillary pressure. The experimental data and predictions are scattered in a similar manner. The scatter arises because in a water-wet system oil is the intermediate-wet phase and its relative permeability is a strong function of saturation history and initial oil saturation [13,14,20]. These predictions are similar to those obtained using a water-wet three-phase network model by Lerdahl *et al.* [18].

Figure 6 illustrates the comparison between predicted and measured three-phase gas relative permeability. Again the predictions are in good agreement with the measured values. At high gas saturation, predictions and experimental data are not very scattered because gas is the most nonwetting phase in a water-wet system, and its relative permeability is a function of only its own saturation. However, the measured values at low gas saturations are quite scattered and this is because of difficulties in the experiments [4,18]. Predicted values at low gas saturation are zero due to finite size effects. This is again similar to the results of Lerdahl *et al.* [18].

Figure 7 presents the comparison between predicted three-phase water relative permeability and measured values. The water relative permeability is slightly overestimated. The reason for this is not known, but it may be due to measurement difficulties. In water-wet systems the water relative permeability is expected to be a function of only its own saturation and similar to two-phase values. Recall that we predict the two-phase water relative permeabilities accurately.

While these results are very encouraging, we are comparing two clouds of points with considerable scatter. In the next section we go one step further and attempt a more rigorous analysis by comparing experiments on a point-by-point basis.

2. Comparison with experiment using saturation tracking

We apply our saturation tracking algorithm presented in Sec. VIII in Ref. [19] to produce identical saturation paths as the measured ones and then compare the predicted and measured relative permeabilities. This is of interest in three-phase flow due to the fact that three-phase macroscopic properties are a strong function of saturation history (path). We analyze two experiments.

Experiment (i). Figure 8 shows the tracked and measured saturation path for a high initial oil saturation experiment (experiment 9, sample 13). The initial point was produced by primary drainage and the saturation tracking algorithm was used to reproduce the experimental path. We were able to reproduce the same path as the experiment.

Figure 9 compares the predicted and measured three-phase oil relative permeability for experiment (i). The prediction compares well with the measured values at high oil saturations but tends to overpredict at low oil saturations. The reason for this is not very clear at this stage but it may be due to scatter in the data, the uncertainty associated with the layer conductance estimations and also the representation of the void space of the rock by idealized angular geometries.

Figure 10 illustrates the comparison between the predicted and measured three-phase gas relative permeability. Due to finite size effects the predicted values at low gas saturations are zero.

Figure 11 compares the predicted three-phase water relative permeability with the measured values. The agreement is fairly good. We slightly overestimate the relative permeability, as discussed in the previous section.

Experiment (ii). Figure 12 shows the measured and tracked saturation paths for another high initial oil saturation experiment (experiment 10, sample 14). Again the initial oil saturation is established by primary drainage.

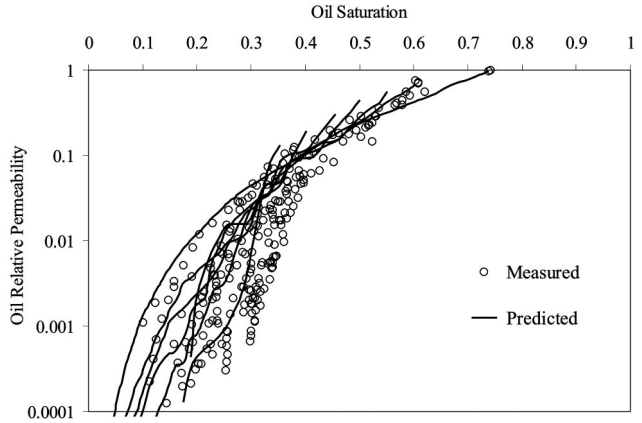

FIG. 5. Comparison of measured [4] and predicted three-phase oil relative permeability during gas injection.

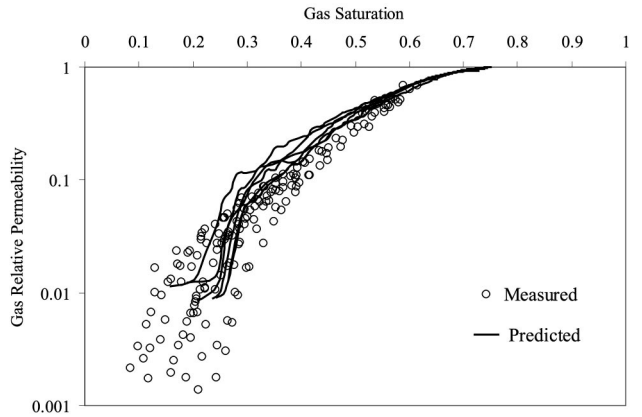

FIG. 6. Comparison of measured and predicted three-phase gas relative permeability during gas injection.

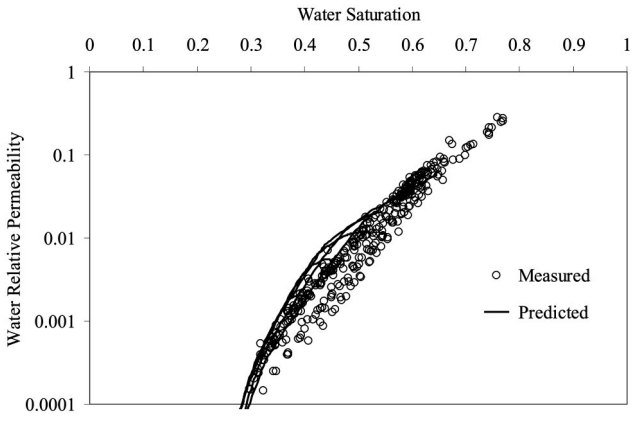

FIG. 7. Comparison of measured and predicted three-phase water relative permeability during gas injection.

Figure 13 compares the predicted and measured three-phase oil relative permeability. Similar to the previous experiment predicted values at low oil saturations are overestimated. This is the region where oil relative permeability is controlled by flow of oil through the layers. The sensitivity of the oil relative permeability to oil layer conductance was tested by multiplying the layer conductance by constant factors of 0.08 and 0.001. The effect is significant, Fig. 13, and indicates that the predicted oil relative permeability is very sensitive to how layer flow is modeled.

Figure 14 indicates the very good agreement between predicted and measured three-phase gas relative permeability. Variations in the oil layer conductance does not have any impact on the gas relative permeability. Gas flows in the center of the larger pores and throats as it is the most nonwetting phase and is unaffected by oil layers.

We analyzed other experiments for both secondary (after primary drainage) and tertiary (after water flooding) gas injection. In all cases the results were similar to those shown here. The predictions of gas and water relative permeabilities were good, and we predicted the oil relative permeability at high saturation accurately. However, at low saturation we systematically overestimated the oil relative permeability. Where we make good predictions, flow is controlled by the subnetworks of pores and throats whose centers are filled with each phase. As we have shown in the two-phase analysis, with a geologically representative network and a range of contact angles that captures the correct balance between pore body filling and snapoff in imbibition, we can predict relative permeability accurately.

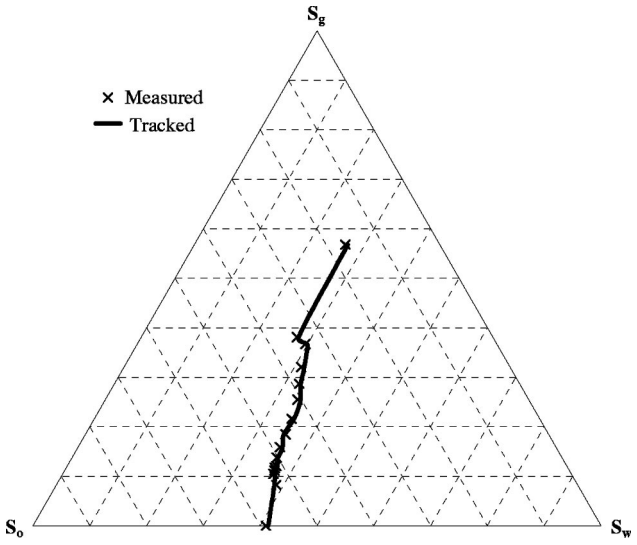

FIG. 8. Comparison of measured and tracked saturation paths for experiment 9, sample 13, of Oak experiments [4].

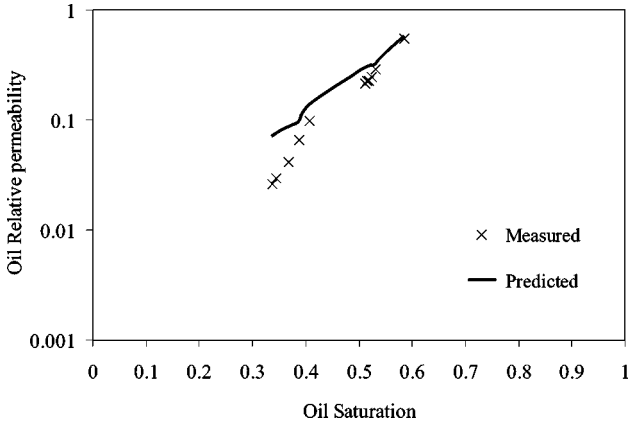

FIG. 9. Comparison of measured and predicted three-phase oil relative permeabilities for experiment 9, sample 13, of Oak experiments [4].

However, the oil relative permeability in gas injection for oil saturations below approximately 0.5 is controlled by oil layers—these layers provide connectivity of the oil phase and without them the oil would be completely trapped at a saturation of around 0.2. This is a situation unique to three-phase flow. It would appear that we significantly overestimate the layer conductance. This is probably because our simplistic representation of connected layers in a corner fails to capture parts of the pore space where the layers are much less stable or conductive.

III. SIMULATION OF DIFFERENT PROCESSES

We now use our model to study different cases that have not necessarily been studied experimentally. We consider

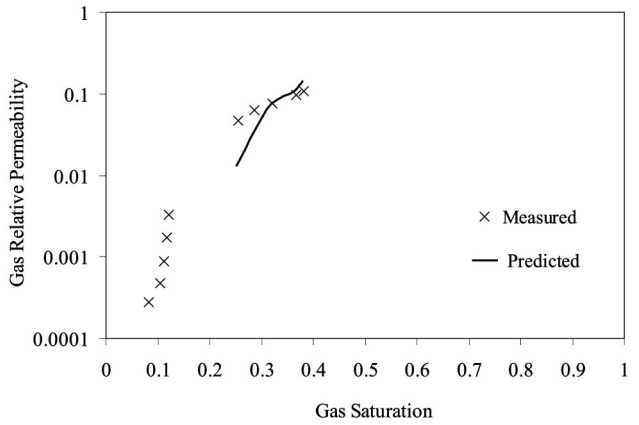

FIG. 10. Comparison of measured and predicted three-phase gas relative permeabilities for experiment 9, sample 13, of Oak experiments [4].

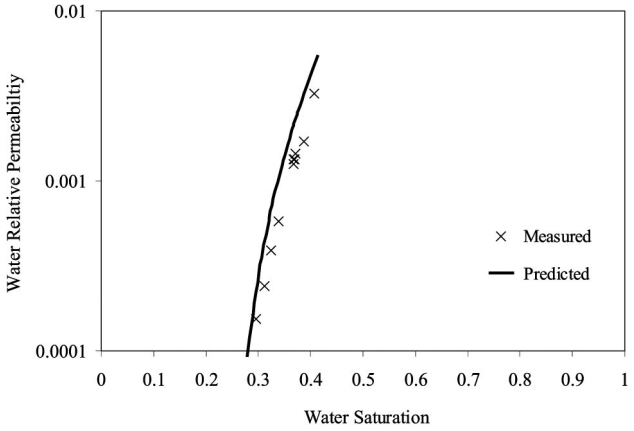

FIG. 11. Comparison of measured and predicted three-phase water relative permeabilities for experiment 9, sample 13, of Oak experiments [4].

two systems with different wettability whose contact angles are tabulated in Table III. We use the same interfacial tensions as before—Table I.

A. Secondary gas injection

Here we simulate gas injection into different initial oil saturations S_{oi} after primary drainage (secondary gas injection) assuming a fixed oil-water capillary pressure. In this section we consider the water-wet system A in Table III. Figure 15 presents the saturation paths taken by each simulation. Since the gas-oil interfacial tension is lower than that of the gas-water, gas displaces oil first and then at the residual or trapped oil saturation (close to zero), it starts displacing water.

Figure 16 compares the three-phase oil relative permeability for secondary gas injection with different initial oil saturations. At high oil saturations, the higher the initial oil saturation, the lower the oil relative permeability. Initially oil

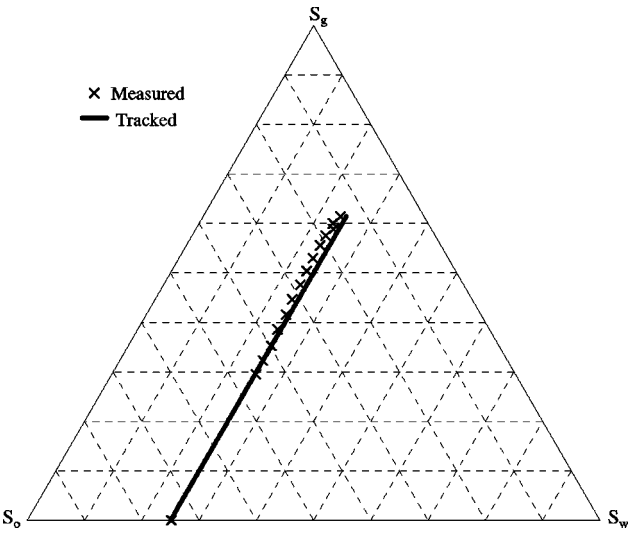

FIG. 12. Comparison of measured and tracked saturation paths for experiment 10, sample 14, of Oak experiments [4].

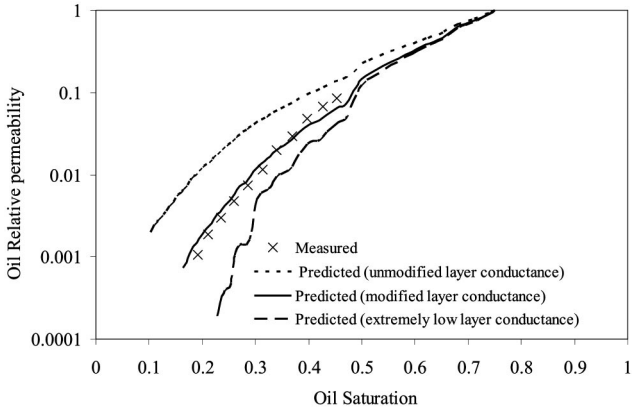

FIG. 13. Comparison of measured and predicted three-phase oil relative permeabilities for experiment 10, sample 14, of Oak experiments [4].

occupies the largest elements. Gas then invades the oil-filled pores and throats in decreasing order of size. For a low initial oil saturation, oil only occupies large elements giving a larger relative permeability than for a high initial oil saturation where oil remains in small elements [13,14,20]. However, at low oil saturations, the higher the initial oil saturation, the higher the oil relative permeability. This is due to the effect of initial oil saturation on oil layer stability. At high initial oil saturations the oil-water capillary pressure, or oil pressure, is high. Oil pushes water far into the corners in configuration group F (see Fig. 7 in Ref. [19]). For low S_{oi}, the oil-water capillary pressure is lower, water occupies more of the corners and oil layers are thinner. Thicker layers have a larger conductance and will collapse later in the displacement, leading to higher oil relative permeabilities.

Since the system is water wet, gas and water relative permeabilities are a function of only their own saturations—water occupies the smallest elements while gas occupies the largest elements—regardless of the initial oil saturation.

B. Comparison of secondary and tertiary gas injection

Here we compare secondary with tertiary gas injection again for the water-wet system A, Table III. Figure 17 shows

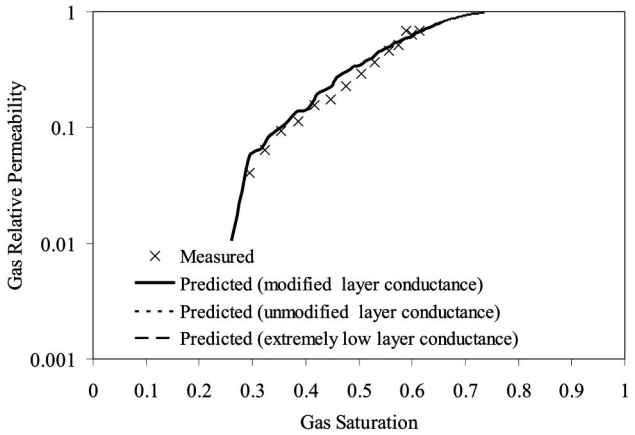

FIG. 14. Comparison of measured and predicted three-phase gas relative permeabilities for experiment 10, sample 14, of Oak experiments [4].

TABLE III. Contact angles (degrees) used to simulate different processes.

System	$\theta_{ow}^{Primary\ Drainage(PD)}$	θ_{gw}^{PD}	θ_{ow}^{r}	θ_{ow}^{a}	θ_{go}^{r}	θ_{go}^{a}	θ_{gw}^{r}	θ_{gw}^{a}
A	0	0	10–50	30–70	0	0	8.46–41.9	25.3–58.1
B	0	0	90–160	110–180	0	0	73.5–112.9	87.8–115.6

the three-phase oil relative permeability for secondary and tertiary gas injection into an initial oil saturation of 0.55. The oil relative permeability for secondary gas injection is not very different from tertiary gas injection at high oil saturations where layer flow is not dominant. At low oil saturations, oil flows mainly through layers. Theses layers are thicker and more stable during secondary gas injection due to the higher oil-water capillary pressure in comparison with tertiary gas injection where the oil layers are thinner and less stable because the oil-water capillary pressure is lower after water flooding. This gives higher oil relative permeabilities for secondary gas injection than for tertiary gas injection with the same initial oil saturation.

In Fig. 17 at high oil saturation we see, approximately, $k_{ro} \propto S_o^4$. The oil relative permeability is controlled by the network of pores and throats filled with oil in the centers and it drops rapidly with oil saturation as this network becomes less well connected. For secondary gas injection, at an oil saturation approximately equal to the water flood residual, we see a crossover to a layer drainage regime where approximately $k_{ro} \propto S_o^2$. This is easily explained theoretically [1,22,30,31]. The hydraulic conductance of the layers is proportional to the square of the cross-sectional area of oil (see Appendix B in Ref. [19]). When most oil is flowing in layers, the oil saturation is proportional to the oil area, leading to the quadratic relative permeability. This behavior has been observed in gas injection and gravity drainage experiments [1,30–32]. Notice that the apparent log-log slope at low saturation is slightly larger than 2, as seen for sandstones [1,32]. This is because some small throats are still oil filled in the layer drainage regime and when they are occupied by gas, their contribution to the oil relative permeability drops significantly. For tertiary gas injection, this oil layer drainage regime is not observed—this is because oil layers collapse during the displacement leading to very low oil relative permeabilities.

The three-phase gas (Fig. 18) and water (Fig. 19) relative permeabilities are the same in secondary and tertiary gas injection. Again this is because they depend on only their own saturations and are relatively insensitive to saturation path, as long as it is a drainage-dominated displacement.

C. Tertiary gas injection into water flood residual oil

The physics involved with gas injection into water flood residual oil is very complex. Several micromodel experiments [33–44] have shown that when gas is injected into such a spreading system the two phenomena of *double displacement* and oil *layer formation* make the initially trapped oil continuous which allows it to drain to very low saturation. This in turn involves coalescence, formation and breakup of trapped clusters of oil. We have implemented these mechanisms in our model and Figs. 20, 24, and 25 show the three-phase oil, water, and gas relative permeabilities for this process again in our water-wet system, A. The oil relative permeability is zero at the end of water flooding (beginning of gas injection) as all the oil is trapped, but it jumps to a nonzero value as it gets reconnected during the early stages of gas injection. This happens at low gas saturation, see Fig. 26, where the trapped oil saturation is plotted against gas saturation.

Figure 20 also compares the oil relative permeability of the tertiary gas injection with that of secondary gas injection with a similar initial oil saturation (S_{oi}=0.38). At high oil saturations, the oil relative permeability for the tertiary case

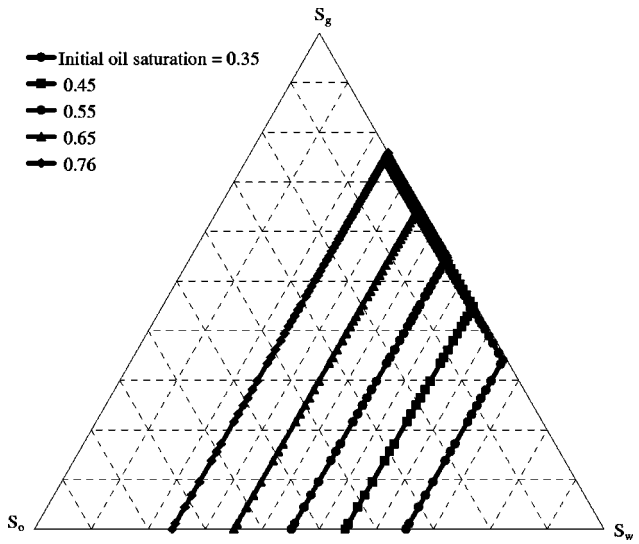

FIG. 15. Saturation paths for secondary gas injection with different initial oil saturations in a spreading system.

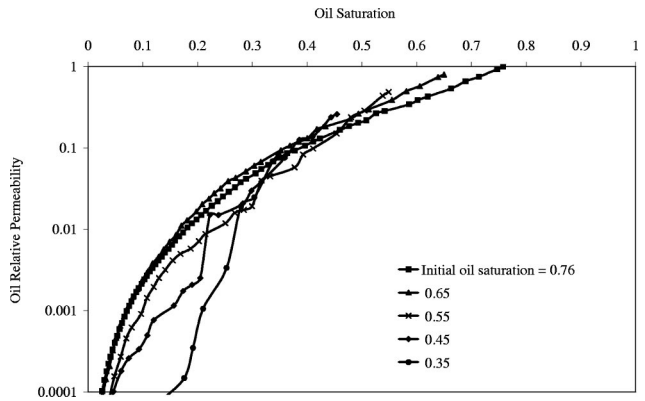

FIG. 16. Three-phase oil relative permeabilities for secondary gas injection with different initial oil saturations.

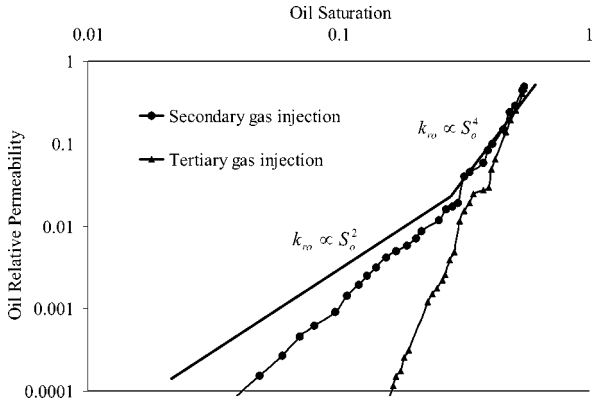

FIG. 17. Comparison of three-phase oil relative permeability for secondary and tertiary gas injection with an initial oil saturation of 0.55.

is lower than that for secondary gas injection. This is because at the beginning of secondary gas injection all the oil resides in the large pores and throats; see Fig. 21, while at the beginning of the tertiary gas injection some of the oil stays in the small elements due to trapping during water flooding; see Fig. 22. In other words, the fraction of large oil filled elements at the starting point of secondary gas injection is larger than for the tertiary case, leading to lower oil relative permeabilities for tertiary gas injection. However, at low oil saturations when layer flow is dominant, the oil relative permeability for tertiary gas injection is higher since, during the displacement, double drainage causes an increase in oil-water capillary pressure making oil layers thicker and more conductive.

Figure 22 shows the pore and throat occupancy at the end of water flooding. The trapped oil resides in the larger elements. During gas injection, double displacement causes the oil to be pushed into smaller pores and throats while the gas occupies the larger elements; see Fig. 23. The oil is now connected, since it also resides in layers in gas-filled elements. This allows oil to be displaced and results in a nonzero oil relative permeability; Fig. 20.

Figure 24 shows the gas relative permeability compared to an equivalent secondary gas injection (S_{oi}=0.38). The gas

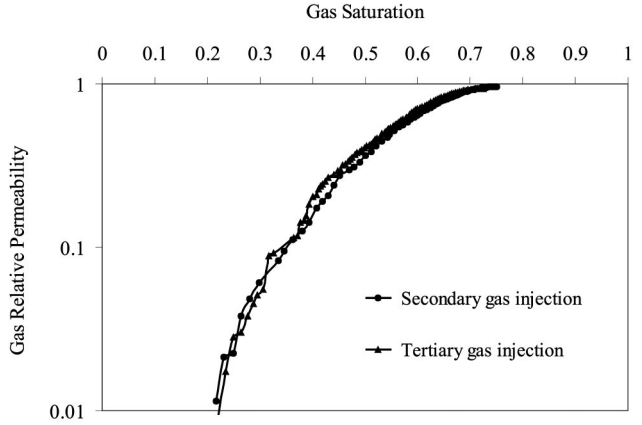

FIG. 18. Comparison of three-phase gas relative permeability for secondary and tertiary gas injection with an initial oil saturation of 0.55.

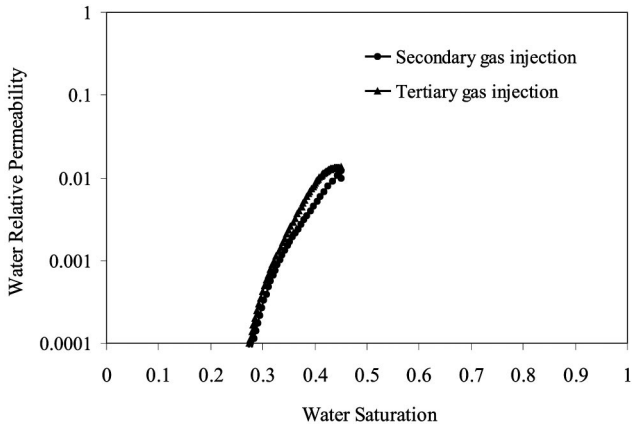

FIG. 19. Comparison of three-phase water relative permeability for secondary and tertiary gas injection with an initial oil saturation of 0.55.

relative permeability for the tertiary case is lower, in contrast to Fig. 18. The reason is that here the oil is trapped and gas is displacing oil by double displacement and hence is less well connected—the trapped oil is blocking the larger pores and throats. Similarly the tertiary water relative permeability is lower; Fig. 25. During the displacement, double drainage causes an increase in oil-water capillary pressure giving a drainage-type displacement for water, pushing it into smaller elements. This is not seen if oil is initially well connected; see Fig. 19.

Table IV shows the displacement statistics for tertiary gas injection into water flood residual oil (S_{oi}=0.384) compared to secondary gas injection with a similar initial oil saturation (S_{oi}=0.38). In tertiary gas injection there is a significant amount of double displacement and oil layer formation that reconnects the oil and rearranges its occupancy (Fig. 23). In contrast, secondary gas injection is controlled by direct gas-oil displacement alone since the oil is initially already connected. At the end of water flooding there were 1864 trapped clusters of oil and during tertiary gas injection into water flood residual oil 507 coalescence, 90 break, and 1040 reconnection events took place (see Fig. 26).

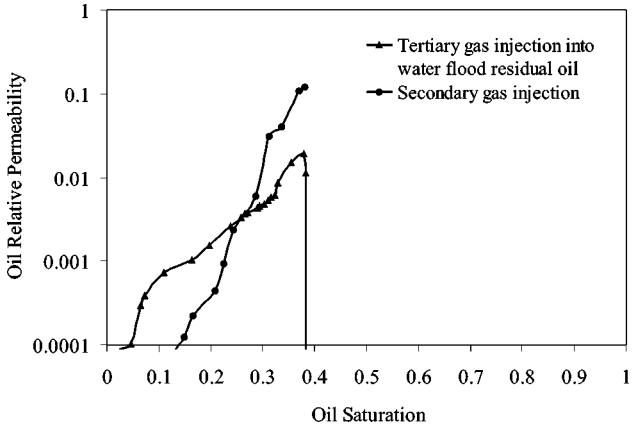

FIG. 20. Three-phase oil relative permeability for tertiary gas injection into water flood residual oil (S_{oi}=0.384) and for secondary gas injection with a similar initial oil saturation (S_{oi}=0.38).

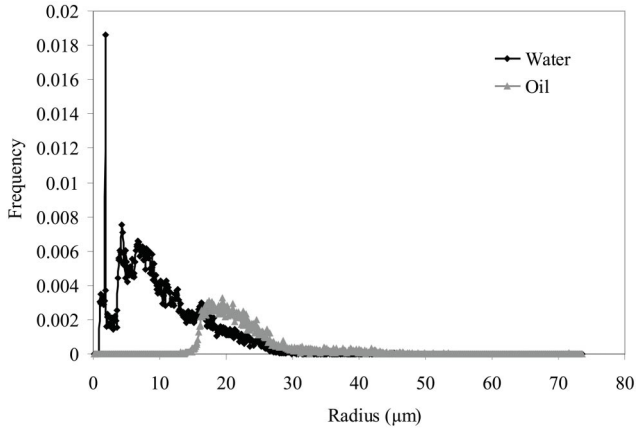

FIG. 21. Pore and throat occupancy as a function of size after primary drainage ($S_o = 0.38$).

D. Effects of wettability

We will now use our model to predict the effect of wettability on three-phase relative permeabilities. In this case, we do not have experimental data to compare against, but the success of network modeling predictions for mixed-wet two-phase systems [24,45] and water-wet two- and three-phase systems gives us some confidence that our results are valid. We compare two cases: water-wet *A* and oil-wet *B* where the distribution of advancing oil/water contact angle is uniform between 30°–70° and 110°–180°, respectively (Table III). Again the interfacial tensions are given in Table I.

We consider primary drainage to irreducible water saturation followed by water flooding to $S_w = 0.4$ ($S_{oi} = 0.6$). Then gas is injected at a constant oil-water capillary pressure.

Figure 27 shows the oil relative permeability. In the oil-wet case, oil remains in smaller pores and throats after water flooding than for a water-wet medium, giving a lower relative permeability. This is seen in Fig. 27 for oil saturations larger than approximately 0.4. At lower oil saturations, gas has invaded most of the oil-filled elements. The relative permeability is limited by the connectivity of the oil phase. In the water-wet medium, oil layers collapse during gas injection, whereas oil layers remain stable throughout the displacement for the oil-wet case. A higher gas pressure is required to collapse oil layers, since water is pinned in the corners—configurations $F-3$ and $F-4$ in Fig. 7 in Ref. [19]. Thus the oil-wet oil relative permeability is larger at low oil saturation.

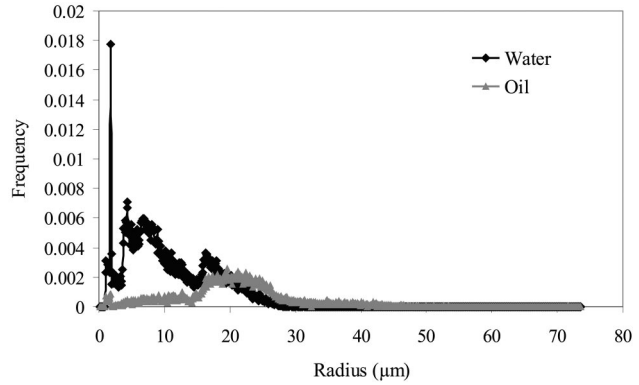

FIG. 22. Pore and throat occupancy as a function of size after water flooding. The trapped oil resides in the larger elements.

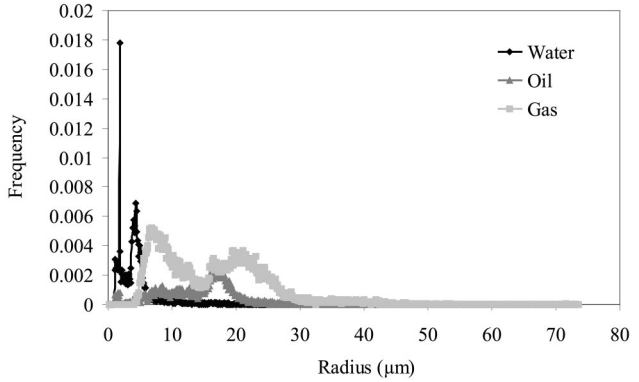

FIG. 23. Pore and throat occupancy as a function of size during tertiary gas injection into water flood residual oil when $S_o \approx 0.16$. Double displacement shifts the oil into intermediate-sized elements.

The water-wet gas relative permeability in Fig. 28 is larger than the oil-wet case at high gas saturation. In a water-wet medium, the gas always occupies the largest pores and throats. For an oil-wet system, gas is not the most nonwetting phase in the presence of water (in Table III some values of θ_{gw} are greater than 90°) and will displace water from some of the smaller pores, resulting in poorer connectivity and conductance. This effect of wettability has been discussed previously [20] and is well established experimentally [30,31,46]. This result is a direct consequence of the constraint on contact angles; Eq. (1) [47].

The water relative permeability in Fig. 29 is at first sight surprising. One might expect that the water relative permeability for the oil-wet case to be higher than for the water-wet medium, since water can be nonwetting to both oil and gas in oil-wet systems, occupying the larger pore spaces. The explanation is that during water flooding water invades the larger pores and throats in the oil-wet medium. This results in an increase in water saturation, but the oil-wet water-filled elements fail to span the network, meaning that the water

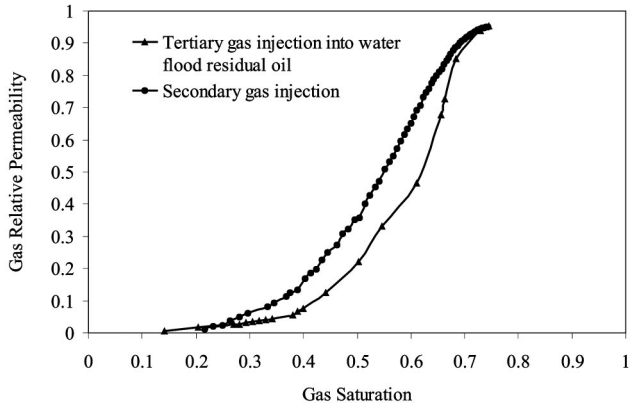

FIG. 24. Three-phase gas relative permeability for tertiary gas injection into water flood residual oil ($S_{oi} = 0.384$) and for secondary gas injection with a similar initial oil saturation ($S_{oi} = 0.38$).

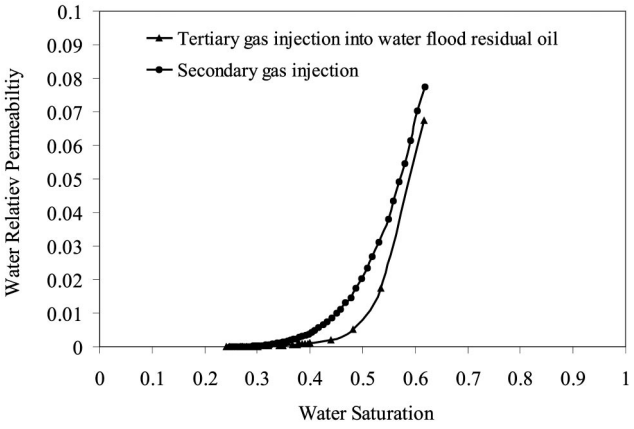

FIG. 25. Three-phase water relative permeability for tertiary gas injection into water flood residual oil (S_{oi}=0.384) and for secondary gas injection with a similar initial oil saturation (S_{oi}=0.38).

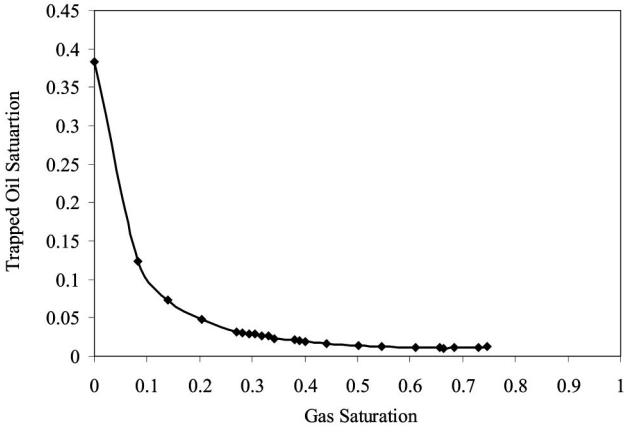

FIG. 26. Trapped oil saturation as a function of gas saturation during tertiary gas injection into water flood residual oil.

relative permeability remains very low. During gas injection, since gas displaces water, the water relative permeability can only decrease from its already negligible value.

IV. CONCLUSIONS

The model successfully predicted two-phase water-wet relative permeabilities measured on Berea sandstone by Oak [4]. For primary drainage there were no parameters to adjust. For oil-water and gas-oil imbibition the advancing contact angles were chosen to match the residual nonwetting phase saturation. Using these contact angles excellent agreement between experiment and predictions was made. For gas-water data we used a constraint, Eq. (1), to predict the gas-water contact angles from the oil-water and gas-oil results. Again the match to experiment was excellent.

We then predicted three-phase gas injection relative permeabilities from Oak [4]. We used a saturation tracking algorithm to follow exactly the same displacement path as in the experiments. The predictions of gas and water relative permeabilities and the oil relative permeability at high oil saturation were good. However, at low oil saturations, where flow is dominated by spreading layers, we systematically overpredicted the oil relative permeability. This was likely to be due to us overestimating the oil layer conductance.

We computed relative permeabilities for cases that had not been studied experimentally. We showed that the oil relative permeability in tertiary gas injection—after water flooding—is lower than in secondary gas injection—after primary drainage, since oil layers are less stable and thinner due to a low initial oil-water capillary pressure. For secondary gas injection we observed an approximately quadratic variation of oil relative permeability with oil saturation when flow was controlled by layers, as seen experimentally. We then compared relative permeabilities of a tertiary gas injection into water flood residual oil with those of a secondary

TABLE IV. The number of different types of displacement for tertiary gas injection into water flood residual oil (S_{oi}=0.384) and for secondary gas injection with a similar initial oil saturation (S_{oi}=0.38).

	Number of displacements	
Displacement type	Tertiary gas injection	Secondary gas injection
Double displacement gas-oil (pistonlike)	1345	0
Double displacement oil-water (pistonlike)	3856	0
Direct gas-oil (pistonlike)	13699	10091
Direct gas-water (pistonlike)	22688	27804
Oil layer collapse	6178	8640
Oil layer formation	1356	0

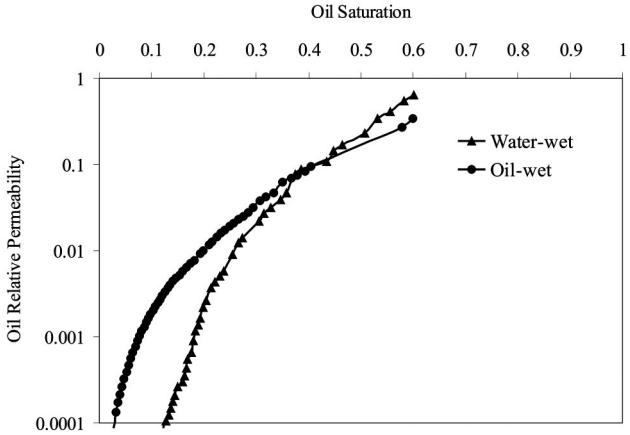

FIG. 27. Effects of wettability on three-phase oil relative permeability. Curves for tertiary gas injection into a water-wet and oil-wet system with initial oil saturation of 0.6 are shown.

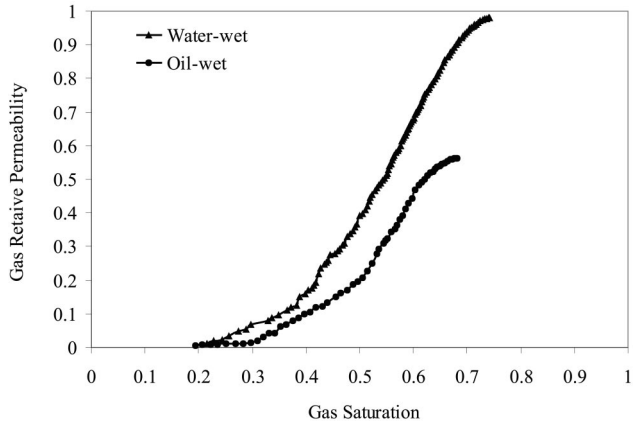

FIG. 28. Effects of wettability on three-phase gas relative permeability. Curves for tertiary gas injection into a water-wet and oil-wet system with initial oil saturation of 0.6 are shown.

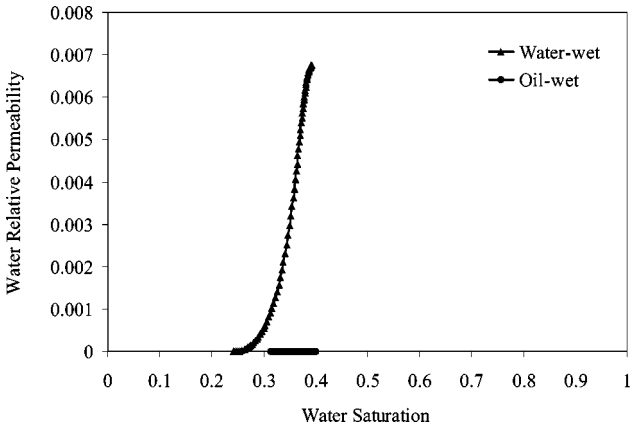

FIG. 29. Effects of wettability on three-phase water relative permeability. Curves for tertiary gas injection into a water-wet and oil-wet system with initial oil saturation of 0.6 are shown.

gas injection with a similar initial oil saturation. The oil relative permeability of the tertiary case was nonzero and higher than that of the secondary gas injection at low oil saturations since double displacement caused an increase in oil-water capillary pressure—in tertiary gas injection—leading to thicker and more conductive oil layers. The increase in the oil-water capillary pressure also lowered the gas and water relative permeabilities for the tertiary case compared to their secondary counterparts. These results were different from tertiary gas injection into oil that was initially already connected. We also showed the effects of wettability on relative permeability by comparing tertiary gas injection relative permeabilities for water-wet and oil-wet systems. The behavior of all three relative permeabilities was different from that observed in two-phase flow and was explained in terms of the pore-scale physics.

The model could now be used to study a wide range of other phenomena in three-phase flow, including water alternate gas (WAG) flooding and gas gravity drainage.

ACKNOWLEDGMENTS

The members of the Imperial College Consortium on Pore-Scale Modeling (BHP, Enterprise, Gaz de France, JNOC, PDVSA-Intevep, Schlumberger, Shell, Statoil, the U.K. Department of Trade and Industry, and the EPSRC) are thanked for their financial support. We also thank Pål-Eric Øren (Statoil) for sharing his Berea network data with us and also for his valuable comments. We thank Gary Jerauld (BP) for providing the Oak data in electronic form and Ken Sorbie (Heriot-Watt University) for his insightful comments on this work.

[1] D. H. Fenwick and M. J. Blunt, SPEJ **3**(1), 86 (1998).
[2] D. H. Fenwick and M. J. Blunt, Adv. Water Resour. **21**(2), 121 (1998).
[3] A. S. Grader and D. J. O'Meara, Proceedings of the 63rd SPE Annual Technical Conference and Exhibition, Houston, TX, 1988, Paper SPE 18293 (unpublished).
[4] M. J. Oak, Proceedings of the SPE/DOE Seventh Symposium on Enhanced Oil Recovery, Tulsa, OK, 1990, Paper SPE 20183 (unpublished).
[5] M. C. Leverett and W. B. Lewis, Trans. Am. Inst. Min., Metall. Pet. Eng. **142**(107), 107 (1940).
[6] L. E. Baker, Proceedings of the SPE/DOE Enhanced Oil Recovery Symposium, Tulsa, OK, 1988, Paper SPE 17369 (unpublished).
[7] M. J. Oak, L. E. Baker, and D. C. Thomas, JPT, J. Pet. Technol. **42**(8), 1054 (1990).
[8] J. E. Nordtvedt, E. Ebeltoft, J. E. Iversen, A. Sylte, H. Urkedal, K. O. Vatne, and A. T. Watson, Proceedings of the SPE Annual Technical Conference and Exhibition, Denver, CO, 1996, Paper SPE 36683 (unpublished).
[9] V. Mani and K. K. Mohanty, J. Colloid Interface Sci. **187**(1), 45 (1997).
[10] V. Mani and K. K. Mohanty, SPEJ **3**, 238 (1998).
[11] P. E. Øren, J. Billiotte, and W. V. Pinczewski, Proceedings of the SPE/DOE Symposium in Improved Oil Recovery, Tulsa, OK, 1994, Paper SPE 27814 (unpublished).
[12] G. G. Pereira, W. V. Pinczewski, D. Y. C. Chan, L. Paterson, and P. E. Øren, Transp. Porous Media **24**(2), 167 (1996).
[13] M. I. J. van Dijke, S. R. McDougall, and K. S. Sorbie, Transp. Porous Media **44**(1), 1 (2001).
[14] M. I. J. van Dijke, K. S. Sorbie, and S. R. McDougall, Adv. Water Resour. **24**(3–4), 365 (2001).
[15] M. I. J. van Dijke and K. S. Sorbie, J. Pet. Sci. Eng. **33**(1–3), 39 (2002).
[16] M. I. J. van Dijke and K. S. Sorbie, Transp. Porous Media **48**(2), 159 (2002).
[17] M. I. J. van Dijke and K. S. Sorbie, Phys. Rev. E **66**, 046302(2) (2002).
[18] T. R. Lerdahl, P. E. Øren, and S. Bakke, Proceedings of the SPE/DOE Symposium in Improved Oil Recovery, Tulsa, OK,

2000, Paper SPE 59311 (unpublished).
[19] M. Piri and M. J. Blunt, Phys. Rev. E **71**, 026301 (2005).
[20] M. H. Hui and M. J. Blunt, J. Phys. Chem. B **104**, 3833 (2000).
[21] A. W. Adamson and A. P. Gast, *Physical Chemistry of Surfaces*, 6th ed. (Wiley, New York, 1997).
[22] M. J. Blunt, SPEJ **5**(4), 435 (2000).
[23] T. Firincioglu, M. J. Blunt, and D. Zhou, Colloids Surf., A **155**(2–3), 259 (1999).
[24] P. H. Valvatne and M. J. Blunt, Water Resour. Res. **40**, W07406 (2004).
[25] M. J. Blunt, SPEJ **2**(4), 494 (1997).
[26] G. R. Jerauld and S. J. Salter, Transp. Porous Media **5**(2), 102 (1990).
[27] N. R. Morrow, J. Can. Pet. Technol. **14**(4), 42 (1975).
[28] F. A. L. Dullien, *Porous Media: Fluid Transport and Pore Structure*, 2nd ed. (Academic, San Diego, 1992).
[29] F. E. Bartell and H. J. Osterhoff, Ind. Eng. Chem. **19**, 1277 (1927).
[30] D. A. DiCarlo, A. Sahni, and M. J. Blunt, Transp. Porous Media **39**(3), 347 (2000).
[31] D. A. DiCarlo, A. Sahni, and M. J. Blunt, SPEJ **5**(1), 82 (2000).
[32] A. Sahni, J. Burger, and M. J. Blunt, Proceedings of the SPE/DOE Improved Oil Recovery Symposium, Tulsa, OK, 1998, Paper SPE 39655 (unpublished).
[33] I. Chatzis, A. Kantzas, and F. A. L. Dullien, Proceedings of the 63rd SPE Annual Technical Conference and Exhibition, Houston, TX, 1988, Paper SPE 18284 (unpublished).
[34] A. Kantzas, I. Chatzis, and F. A. L. Dullien, Proceedings of the SPE Rocky Mountain Regional Meeting, Casper, WY, 1988, Paper SPE 17506 (unpublished).
[35] A. Kantzas, I. Chatzis, and F. A. L. Dullien, Proceedings of the SPE/DOE Enhanced Oil Recovery Symposium, Tulsa, OK, 1988, Paper SPE 17379 (unpublished).
[36] P. E. Øren and W. V. Pinczewski, Proceedings of the 6th European IOR Symposium, Stavanger, 1991 (unpublished).
[37] P. E. Øren and W. V. Pinczewski, SPE Form. Eval. **7**, 70 (1992).
[38] P. E. Øren and W. V. Pinczewski, Proceedings of the 67th SPE Annual Technical Conference and Exhibition, Washington, DC, 1992, Paper SPE 24881 (unpublished).
[39] W. E. Soll, M. A. Celia, and J. L. Wilson, Water Resour. Res. **29**(9), 2963 (1993).
[40] P. E. Øren and W. V. Pinczewski, SPE Form. Eval. **9**(2), 149 (1994).
[41] M. J. Blunt, D. Zhou, and D. H. Fenwick, Transp. Porous Media **20**(1–2), 77 (1995).
[42] P. E. Øren and W. V. Pinczewski, Transp. Porous Media **20** (1–2), 105 (1995).
[43] O. Vizika and J. M. Lombard, SPE Reservoir Eng. **11**(1), 54 (1996).
[44] A. A. Keller, M. J. Blunt, and P. V. Roberts, Transp. Porous Media **26**(3), 277 (1997).
[45] M. D. Jackson, P. H. Valvatne, and M. J. Blunt, J. Pet. Sci. Eng. **39**(3–4), 231 (2003).
[46] J. C. Moulu, O. Vizika, P. Egermann, and F. Kalaydjian, Proceedings of the SPE Annual Technical Conference and Exhibition, Houston, TX, 1999, Paper SPE 56477 (unpublished).
[47] M. J. Blunt, J. Colloid Interface Sci. **239**(1), 281 (2001).